

This work was written as part of one of the author's official duties as an Employee of the United States Government and is therefore a work of the United States Government. In accordance with 17 U.S.C. 105, no copyright protection is available for such works under U.S. Law.

Public Domain Mark 1.0

<https://creativecommons.org/publicdomain/mark/1.0/>

Access to this work was provided by the University of Maryland, Baltimore County (UMBC) ScholarWorks@UMBC digital repository on the Maryland Shared Open Access (MD-SOAR) platform.

Please provide feedback

Please support the ScholarWorks@UMBC repository by emailing scholarworks-group@umbc.edu and telling us what having access to this work means to you and why it's important to you. Thank you.

PROCEEDINGS OF SPIE

[SPIDigitalLibrary.org/conference-proceedings-of-spie](https://spiedigitallibrary.org/conference-proceedings-of-spie)

Seasonal variation of UV radiation in the ocean under clear and cloudy conditions

Ziauddin Ahmad, Jay Herman, Alexander Vasilkov, Maria Tzortziou, B. Mitchell, et al.

Ziauddin Ahmad, Jay R. Herman, Alexander P. Vasilkov, Maria Tzortziou, B. Gregory Mitchell, Mati Kahru, "Seasonal variation of UV radiation in the ocean under clear and cloudy conditions," Proc. SPIE 5156, Ultraviolet Ground- and Space-based Measurements, Models, and Effects III, (4 November 2003); doi: 10.1117/12.505298

SPIE.

Event: Optical Science and Technology, SPIE's 48th Annual Meeting, 2003, San Diego, California, United States

Seasonal variation of UV radiation in the ocean under clear and cloudy conditions

Z. Ahmad^{*a}, J. R. Herman^b, A. Vasilkov^c, M. Tzortziou^d, G. Mitchell^e, M. Kahru^e

^aScience and Data Systems, Inc., Silver Spring, MD 20906

^bNASA/Goddard Space Flight Center, Code 916, Greenbelt, MD 20771

^cScience Systems and Applications, Inc., 10210 Greenbelt Road, Lanham, MD 20706

^dUniversity of Maryland, College Park, MD 20742

^eScripps Institution of Oceanography, University of California San Diego, La Jolla, CA 92093

ABSTRACT

Seasonal variability of solar UV radiation in ocean waters is estimated on a global scale by combining satellite measurements of scene reflectivity (TOMS), column ozone (TOMS) and chlorophyll concentration (SeaWiFS) with radiative transfer calculations for an ocean-atmosphere system. The new features are an extension of underwater radiative transfer (scattering and absorption) into the UV, inclusion of polarization in the above water diffuse radiances, the proper treatment of Fresnel reflection, and first order atmospheric backscatter of water-leaving radiance to the oceans. Maps of downwelling diffuse irradiances (E_d) at ocean surface and at different depths in the ocean, diffuse attenuation coefficient (K_d), and ten percent penetration depth (Z_{10}) of solar irradiation are computed for open ocean waters. Results on spectral irradiances at 310 nm in UV-B and at 380 nm in UV-A part of the spectrum are presented with particular emphasis on the role of aerosols, clouds, and ozone in the atmosphere and chlorophyll concentrations in the ocean.

Keywords: UV radiation, column ozone amount, chlorophyll concentration, radiative transfer, UV irradiance in ocean, UV penetration depth in ocean.

INTRODUCTION

UV radiation (UVR) at the Earth's sea level is identified with the wavelength range of 280 to 400 nm. Solar radiation impinging at the top of the atmosphere that is shorter than 280 nm is almost totally absorbed by ozone in the stratosphere while wavelengths longer than 320 nm are partially attenuated by molecular scattering, aerosol scattering and absorption, and by clouds. Interest in UVR reaching the Earth's surface and at different depths in the ocean has increased considerably since the discovery of ozone hole and its relationship to anthropogenic activity. A number of investigators including, Herman et al.^{1,2}, Mora et al.³, and Arrigo et al.⁴, have shown that the increased level of biologically active UV-B radiation due to the depletion of Earth's ozone layer affects both the land and aquatic ecosystems. There is no consensus on the magnitude of the ozone-depletion effect on ocean biology and productivity. Smith et al.⁵ have reported a loss of 6-12% in biological productivity while, Neale et al.^{6,7} and Holm-Hansen et al.⁸ reported a decrease of 5%, and Arrigo⁹ reported a decrease of 1%. In addition to changing the amount of carbon sequestration in the ocean, increase in UV-B radiation generally increase the photochemical production of the greenhouse gas carbonyl sulfide (COS) in seawater (Zepp and Andreae¹⁰) causing changes in long-term global biogeochemical cycles. While a heat trapping greenhouse gas in the troposphere, COS can be dissociated to form stratospheric sulfate particles (Crutzen¹¹ and Engel and Schmidt¹²) and contribute to atmospheric cooling (Charlson et al.¹³). The net balance of these competing effects is not well known.

To quantify the effects of UV radiation on aquatic organisms on a global scale, one needs an estimate of the in-water radiation field, which in turn depends on the solar irradiation reaching the surface through the atmosphere. A number of authors, for example, Krotkov et al.^{14,15}, Herman et al.^{16,17}, Eck et al.¹⁸ have shown that UV radiation reaching the Earth surface can be determined from satellite measurements with an accuracy comparable to the ground base measurements. The advantage of the satellite method is that remote areas, inaccessible to ground-based

* ahmad@qhearts.gsfc.nasa.gov; phone 1 301 614 6819

measurements, can be monitored for the amount of solar radiation reaching the surface at all wavelengths. This is especially true over the oceans where it has been shown that there are large variations in incident UV radiation as a function of latitude and longitude, as well as major inter-hemispheric differences for the same latitude and season (Herman et al.¹⁷).

Recently, we have developed a complete ocean-atmosphere radiative transfer program by combining our extension to the Hydrolight code (Mobley¹⁹) to 290 nm wavelength with a vector (polarization) atmospheric code with a rough ocean surface at the base of the atmosphere (Ahmad and Fraser²⁰). The combined code incorporates the effects of aerosols, clouds, ozone, molecular scattering, Fresnel surface reflection, wind and wave effects, and ocean absorption and scattering. Vasilkov et al.²¹ have compared the results (K_d) from the newly developed model and reported a favorable comparison with in-situ measurements of Kahru and Mitchell²². They have also found that the calculated and measured radiation field at various depths in the ocean are in significantly better agreement than those obtained by some of the standard approximate methods (e.g., the two-stream method and the Quasi Single-Scattering Approximation, QSSA (Vasilkov et al., present proceeding)). Recent work by Tzortziou (PhD thesis, personal communication) has shown similar agreement in estuarine waters (Chesapeake Bay).

In this study, we have used our new ocean-atmosphere model to investigate the seasonal variability of the under water UV irradiances under clear, and cloudy atmospheric conditions. The following sections describe the details our computational methodology and the results of our model calculations.

2.0 COMPUTATIONAL METHODOLOGY

Our method to compute the UV irradiances in the ocean is based on a look-up table approach. We used three sets of look-up tables for this purpose. Two of these tables were used to compute irradiances reaching the ocean surfaces: One for cloud-free condition and the other for cloudy conditions. Both tables include the effects from backscattering of water leaving radiances, and Fresnel surface reflection on the net downwelling radiances. Once the downwelling radiances on the ocean surface were determined, the third table was used to compute upward and downward irradiances at different depths in the ocean. For this study, we performed radiative transfer simulations at 2nm intervals in the UV-B (290-320 nm), and at 5nm interval in the UV-A (320-400 nm) part of the spectrum. In all, there were 32 spectral intervals or bands. The details of the table generation and over-all computational strategy are described below.

2.1 Look Up Tables For Cloud-Free Atmosphere

For cloud-free conditions, our model atmosphere consisted of the standard atmospheric gases (N_2 , O_2), aerosols, and ozone. The marine aerosols were distributed vertically according to Air force Geophysical Laboratory distribution (AFGL²³) for 23 km visibility. We used a bi-modal lognormal distribution to characterize the aerosols. The modal radii for fine and coarse modes were 0.0327 and 0.3180 μm and the standard deviations were 2.239 and 2.512 μm . The radii values were for a humidity value of 80 percent (AFGL²³). The relative weights of the number of particles in the fine and coarse modes were 0.999 to 0.001. We used AFGL aerosol refractive index tables to interpolate the refractive indices of the fine and the coarse particles for the 32 wavelengths of the look tables. In the tables the aerosol optical thickness (τ^a) was defined at 380 nm, and optical thickness at all other wavelengths were determined from the ratio of the extinction coefficients, where the reference coefficient was defined at 380 nm. The ozone distributions were taken from the Total Ozone Mapping Spectrometer (TOMS) Version-7 operational processing of data for mid-latitudes. The ozone amounts were varied from 125 DU to 575 DU in intervals of 50 DU to cover the global range of ozone measured by the TOMS instrument. For purposes of RT calculations, average values of Rayleigh scattering coefficient, ozone absorption coefficient, and extra-terrestrial solar irradiance were computed for each spectral interval. The ozone absorption coefficients were computed for -46°C from the high resolution Bass and Paur²⁴ temperature dependent ozone absorption coefficients, and the band-average values of the extra-terrestrial solar irradiances were derived from the high-resolution SUSIM solar spectra (Brueckner, et al²⁵).

In the RT simulations of downwelling irradiances for cloud-free conditions, we used Cox and Munk's²⁶ wind direction-independent slope probability distribution to characterize the rough ocean surface. In Cox and Munk's distribution, the variance of the slopes of the waves on the ocean surface is linearly related to the wind speed over the ocean surface. We used a wind speed of 6 m/sec to describe the average calm-ocean roughness. Using the wind

direction-independent slope probability distribution substantially reduces the computation time, because it makes the reflection matrix of the rough ocean independent of the azimuth direction (ϕ') of the incident radiation. The RT simulations were carried out with the help of a code called MODRAD (MODified RADtran) developed by Ahmad and Fraser²⁰. The code properly accounts for Fresnel reflection law at the lower boundary and accounts for all orders of scattering and polarization. The RT equation is solved for all the Stokes parameters (I , I_r , U and V) iteratively including the reflecting radiation at the ocean-atmosphere interface back into the atmosphere using a pre-computed reflection matrix for a rough ocean. The MODRAD RT code is very flexible, and can accept any arbitrary aerosol phase matrix as well as aerosol and ozone profiles. Also, the code can be run for any wavelength in UV, visible, or near-IR part of the spectrum.

2.2 Look Up Tables For Cloudy Atmospheres

For cloudy cases, we used tables generated by MODRAD when the effective cloud optical thickness (τ^{cloud}) was determined to be less than 5, while for τ^{cloud} greater than 5, we used the DISORT (DIScreate Ordinate Radiative Transfer) code developed by Stamnes et al.²⁷. The advantage of DISORT is that it is much faster than MODRAD particularly for thick clouds, but, because it is a scalar code and neglects polarization, the radiance calculations needed for the air-ocean interface are less reliable in the UV part of the spectrum. For optically thick clouds ($\tau^{\text{cloud}} \geq 20$) the agreement in radiances between the two codes, MODRAD and DISORT, is better than ~1 percent. We used Deirmendjian's C1 modified gamma distribution (Deirmendjian²⁸) to characterize the cloud droplets. This distribution has been used by a number of investigators to study fair weather cumulus clouds (Hansen²⁹, King and Harshvardhan³⁰, Rossow and Schiffer³¹). In our simulations, the thickness of the cloud layer was ~1.6 km and it was placed between 700 hPa and 850 hPa. The tables were generated by varying the ozone amount, from 125 DU to 575 DU (as in the cloud free case), and varied the cloud optical thickness from 1 to 100 ($\tau^{\text{cloud}} = 1, 3, 5, 7, 10, 15, 20, 30, 50, 100$). The solar zenith angle, θ_0 , was varied from zero to 84°.

2.3 Look Up Tables For Irradiances At Different Depths In The Ocean

To compute the irradiances at different depths in the ocean, we used a modified version of Hydrolight program (Vasilkov et al.³³) coupled to MODRAD. The original program, developed by Mobley¹⁹, was restricted to 400 nm in the visible, and approximated down to 350 nm in the UV part of the spectrum. However, our modified version can be used down to 290 nm. Like DISORT, Hydrolight is a scalar program, that is, it neglects the effect of polarization in the radiative transfer calculations. The modified version accepts the output of MODRAD and DISORT codes (the downwelling radiances and irradiances) as input for radiance and irradiance computations at different depths in the ocean. We used Vasilkov et al.³² parameterization to describe the chlorophyll-specific absorption coefficients in the UV from 290 to 400 nm. For water absorption coefficients, we used Pope and Fry's³³ water absorption coefficients at 380 nm and Quickenden and Irvine³⁴ values from 290 to 320 nm and interpolated the values at the desired wavelength by assuming a linear relationship between water absorption coefficient and wavelength in log-space. For pure sea-water scattering coefficients, we used values given by Smith and Baker³⁵. All the calculations were carried out for Case-1 water where we assumed that the absorption by CDOM co-varies with chlorophyll. To keep the number of computations manageable, lookup tables were generated for only eight values of solar zenith angles (0, 15, 30, 45, 60, 70, 80 degrees) and six values of ozone amounts (225, 325, 425, 525, and 575 DU). Chlorophyll concentration was assumed to be constant with depth and the amount was varied from 0.01 to 10 mg/m³. The irradiances were computed at 2-meter intervals from zero to 20 m depth in the ocean. Other details of the simulations can be found in an accompanying paper by Vasilkov et al. in the present proceeding.

2.4 Global Maps Of UV Irradiances

To construct the global maps of UV irradiances at different depths in the ocean, we first divided the globe into 1° x 1° boxes and used TOMS' daily ozone amount and scene reflectivity values at each grid to compute the irradiance on the ocean surface. Since TOMS is in a Sun-synchronous orbit and crosses the equator near local noon. For each 1° x 1° grid we first computed the solar zenith angle for the local noontime and then examined the TOMS scene reflectivity for the presence of clouds. If the reflectivity value R was less than 10 reflectivity units (RU, where 1 RU is $R=0.01$), we assumed the scene to be cloud free and use MODRAD generated tables. For grids with scene reflectivity greater than 10 RU, we assumed the presence of clouds and depending on the cloud optical thickness, either used the MODRAD generated tables or the DISORT generated tables. For cloud-free grids ($R \leq 10$), we first computed an effective aerosol optical thickness (τ^a) and then interpolated the look-up table for the appropriate solar zenith angle and ozone amount to get the downwelling irradiance and radiances on the ocean surface.

For grids with clouds ($RU > 10$), we first determined an effective cloud optical thickness, τ^{cloud} . If τ^{cloud} was less than 5 then we used MODRAD generated look up tables, otherwise DISORT generated look up tables for cloudy atmospheres. These tables were interpolated for cloud optical thickness, solar zenith angle and ozone amount to get the downwelling irradiance and radiance over the ocean surface. The choice of τ^{cloud} equal to 5 was based on radiative transfer simulations. It was found that for τ^{cloud} greater than 5, the values of downwelling irradiances from the two codes (MODRAD and DISORT) were in good agreement (better than 0.5 %) provided we used a value of 0.055 for Lambertian reflectivity in the DISORT code. To compute the irradiances at various depths in the ocean, we used a monthly chlorophyll concentration climatology produced by the SeaWIFS project and look-up tables were generated by our modified Hydrolight program. The tables were interpolated for ozone amount, solar zenith angle and chlorophyll amount. For the present study only 1998 TOMS and SeaWIFS data were considered. The parameters computed were the monthly average values of downwelling irradiances (E_d) on the ocean surface and at 0, 5, 10, 15, and 20-meter depths in the ocean, the upwelling irradiance just above the ocean surface (E_u), the downwelling irradiance attenuation coefficient (K_d), and the 10 percent attenuation depth (Z_{10}) for each of the 32 spectral bands. The monthly-average values were a mid-month (days 12 to 18) seven-day average value that was labeled as monthly average values.

3.0 RESULTS

3.1 Downwelling Irradiances (E_d) on the Ocean Surface

Our simulation results show that the downwelling irradiances on the ocean surface in the UV-A part of the spectrum are primarily determined by the solar zenith angle and cloudiness. The noontime solar zenith angle at a given grid point is the difference between the latitude of the grid and the solar declination on that particular day. This means that the downwelling irradiance for cloud-free cases will be high in the northern hemisphere and low in the southern hemisphere during the summer months. The overall effect of the clouds is to reflect the downwelling irradiance in approximate proportion to the cloud reflectivity R while reducing the transmission T through the clouds. Although clouds reflect incident radiation anisotropically, Krotkov et al.¹⁵ have shown that $T=1-R$ is a very good approximation for the transmission of irradiance through the cloud. Here, R is the Lambert equivalent reflectivity of the cloud and, in general, depends on the angle of illumination. Figure 1(a) shows the average values of E_d for 380 nm band over the globe for the month of July in the absence of clouds, while Fig. 1(b) shows E_d values in the presence of real clouds. In the 380 nm band the ozone absorption is practically zero. The real cloud reflectivity values for the month of July 1998 as determined by the TOMS instrument are shown in Fig. 1(c). We find that over most of the globe, the cloud reflectivity is generally less than 50 RU and over the northern equatorial Pacific Ocean the reflectivity values are, generally, in the range of zero to 30 RU. Over the same region, (i.e., northern equatorial Pacific Ocean), the irradiance value in the absence of clouds is between 0.9 and 1.05 W/m²/nm (Fig. 1(a)) and in the presence of clouds the irradiance value varies from 0.75 to 1.5 W/m²/nm (Fig. 1(b)). We have also examined the effect of aerosols on the downwelling irradiance on the ocean surface. Radiative transfer simulation results show that for a nominal marine aerosol optical thickness (τ^a) of 0.25 at 380 nm, the total downwelling irradiance decreases by ~3 percent at $\theta_o=30^\circ$ and by 6 percent at $\theta_o=60^\circ$. For the same value of τ^a the decrease at 310 nm is ~3.5 percent at $\theta_o=30^\circ$ and ~5 percent at $\theta_o=60^\circ$. Even though the total reduction by aerosols is much smaller than for clouds, simulation results show that for accurate determination of total downwelling irradiance one must apply an aerosol correction based on table lookup.

Figure 2(a) shows the downwelling irradiances E_d at 310 nm in the presence of clouds and ozone absorption for the month of July 1998. The 310 nm band provides a good representation of the UV-B part of the spectrum, because it has approximately a 1:1 sensitivity to ozone change. Since ozone is generally low at the equator and increases poleward, and ozone absorption increases with solar zenith angle, the effect of ozone will be higher in the mid and the higher latitude than in the tropics.

Downwelling Irrad. (380 nm, JUL_1998, Surf 0+no_clouds)

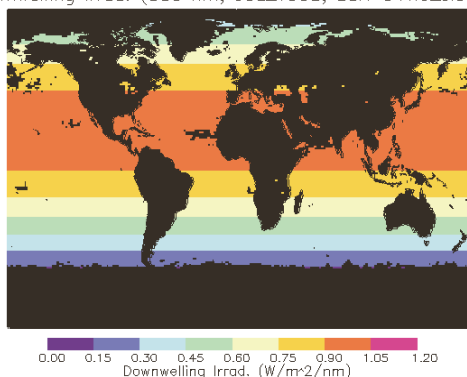


Fig. 1 (a) Downwelling irradiance (E_d (380)) on the ocean surface in the absence of clouds

Reflectivity (JUL_1998)

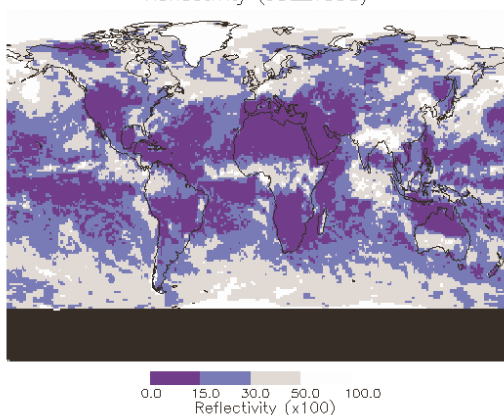


Fig. 1 (c) Average cloud coverage and reflectivity for the month of July 1998.

Ozone Amount(JUL_1998)

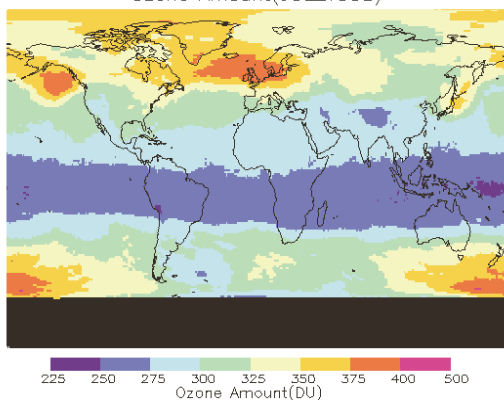


Fig. 2 (b) Average ozone amount for the month of July 1998 from the EP-TOMS instrument.

Downwelling Irrad. (380 nm, JUL_1998, Surf 0+)

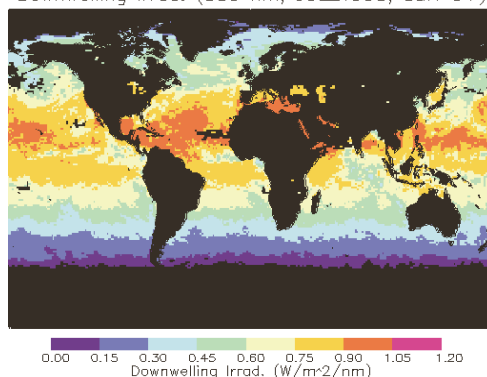


Fig. 1 (b) Downwelling irradiance (E_d (380)) on the ocean surface for the month of July 1998 in the presence of clouds.

Downwelling Irrad. (310 nm, JUL_1998, Surf 0+)

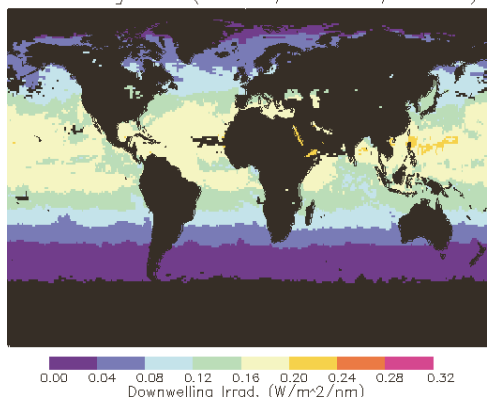


Fig. 2 (a) Downwelling irradiance E_d (310)) on the ocean surface for the month of July 1998 in the presence of ozone and clouds

Chlorophyll (Seawifs,JUL_1998)

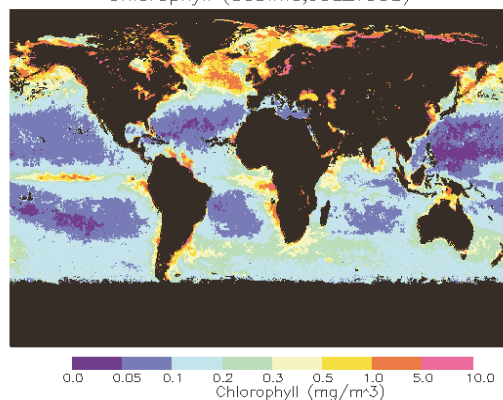
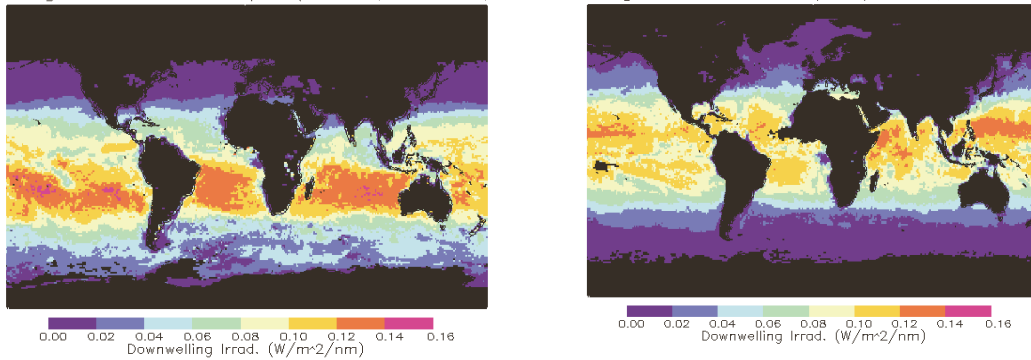


Fig. 2 (c) Average chlorophyll concentration for the month of July from the SeaWiFFs instrument.

Downwelling Irrad at 5 Meter Depth. (310 nm, JAN_1998, 5 m) Downwelling Irrad at 5 Meter Depth. (310 nm, APR_1998, 5 m)



Downwelling Irrad at 5 Meter Depth. (310 nm, JUL_1998, 5 m) Downwelling Irrad at 5 Meter Depth. (310 nm, OCT_1998, 5 m)

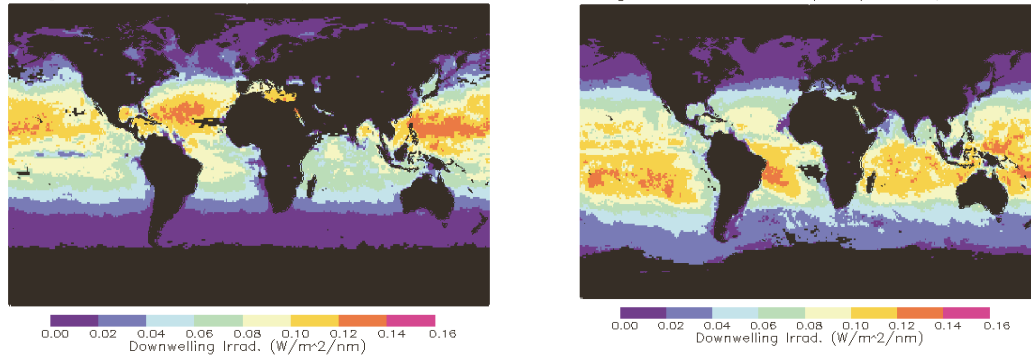


Fig. 2(d-g) Downwelling irradiance at 5 m depth in ocean at 310 nm for the months of January, April, July and October of 1998.

The downwelling irradiance at a 5 meter depth at 310 nm for the months of January, April, July and October, 1998 are shown in Fig. 2(d-g). The irradiance at this depth is primarily determined by the irradiance on the ocean surface modulated by the chlorophyll absorption in the ocean and to a small extent by the Fresnel reflection at the ocean's surface. For example, we find that for the month of July 1998, the overall features of the irradiance distribution in the tropical region in Fig. 2(f) are very similar to those in Fig. 2(d). At the same time, the figure also shows the decrease in irradiance in the equatorial Pacific region due to increase level of chlorophyll as shown in Figure 2(c). The results in Fig. 2(d-g) show increased level of downwelling irradiance (0.12 to $0.16 \text{ W}/\text{m}^2/\text{nm}$) in the southern tropical region of the globe during the month of January than during any other month. This is due to the fact that during January the sub-solar point is in the southern hemisphere so that the noontime solar zenith angle is small and more radiation reaches the ocean surface. Also, the southern tropic region is unique in the sense that there is a large body of ocean where the chlorophyll concentration is very small, and as a result, the higher amounts of incident radiation also penetrates deeper into the ocean. We also find that the band of high irradiance values moves northward during spring and summer and then southward in October following the annual minimum solar zenith angle. At any given place in the map the irradiance value is calculated from the cloud-free case including ozone absorption modulated by cloud reflectivity and chlorophyll in the ocean.

3.2 The Attenuation Coefficient K_d for Downwelling Irradiances in the Ocean

K_d is an apparent optical property (AOP) of water that is highly correlated with ocean chlorophyll concentration and it is a measure of the effective logarithmic decrease of downwelling diffuse irradiance with depth in the ocean. It is relatively insensitive to small changes in the radiation field in the ocean. Approximately 90% of diffuse reflected light from the ocean comes from an ocean depth equal to $1/K_d$. Figures 3(a) and 3(b), respectively, show the global maps of K_d for 380 and 310 nm bands. Both figures show the broad features of chlorophyll concentration shown in Fig. 2(c). However, the K_d values at 380 nm are smaller than K_d values at 310 nm primarily due to higher chlorophyll absorption coefficient at the shorter wavelengths. For example, near southern Iceland in the northern Atlantic Ocean, the K_d (380) is in the range of 0.15 - 0.20 m^{-1} . In the same region the K_d (310) is in the range of 0.35 - 0.50 m^{-1} .

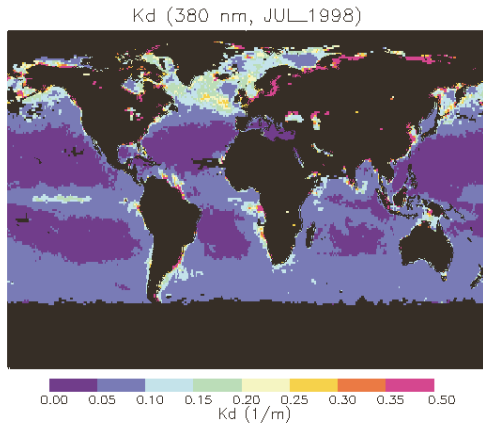


Fig. 3 (a) Diffuse attenuation coefficient K_d (380) for the month of July 1998.

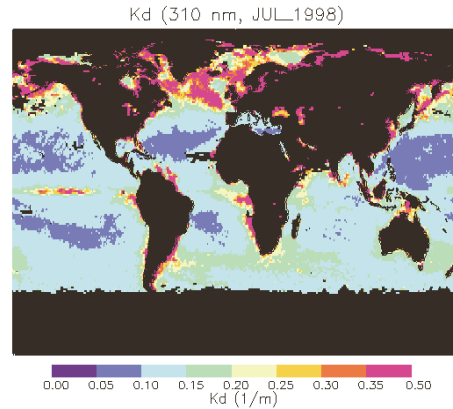


Fig. 3 (b) Diffuse attenuation coefficient K_d (310) for the month of July 1998.

We have compared our computed values of K_d for 310 nm for a few locations with those published in literature (Hojerslev and Aas³⁶). These values are shown in Table 1 for 3 locations in the North Atlantic and Gulf of Mexico. Although Hojerslev and Aas³⁶ data are for a different year, the agreement between the model calculations and the observations is very good and validates the model assumptions and computation details.

Table 1. A comparison of observed and computed $K_d(310)$ values in the North Atlantic and Gulf of Mexico oceanic waters.

Hojerslev and Aas ³⁶			Present Study		
Area	Time	$K_d(310)$	Time	Lat-Long Box	$K_d(310)$
Orkney-Shetland	July 1978	0.39	July 1998	58-60N, 1-3W	0.37 ± 0.04
North of Faroe Island	July 1978	0.15	July 1998	68-69N, 5-6W	0.18 ± 0.01
Gulf of Mexico	Feb-July 1982, 1987, 1988	0.10-0.12	July 1998	24-26N, 91-93W	0.10 ± 0.01

Hojerslev and Aas³⁶ have also shown that in the Norwegian Sea and adjacent waters with low concentration of yellow substance, $K_d(310)$ is highly correlated with $K_d(465)$. Their correlation coefficient for the linear relationship is 0.998. We have examined $K_d(310)$ in terms of $K_d(380)$ for the same location and found a similar linear relationship. This is shown in Fig. 4. In this figure we also show the data points taken from a graph in Diaz et al³⁷ summarizing the work of other investigators. The agreement with the data is quite good considering that the data in Diaz et al³⁷ comes from different types of waters.

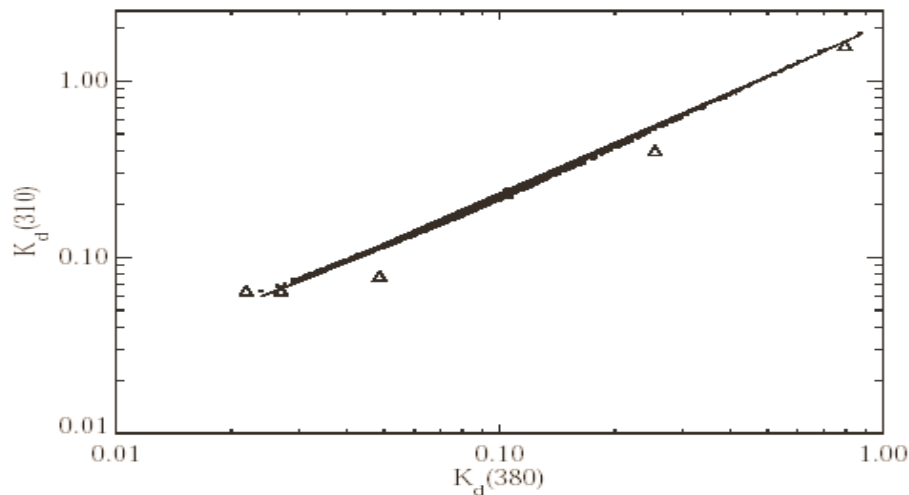


Fig. 4 Relationship between attenuation coefficient $K_d(310)$ in UV-B to attenuation coefficient $K_d(380)$ in UV-A part of the spectrum. The solid line is a least square fit to the data and the triangles are data points taken from a graph in Diaz et al³⁷ summarizing the work of other investigators.

3.3 Z_{10} Penetration Depth

The ten percent irradiance penetration depth (Z_{10}) is a useful indicator of the maximum depth limit for UV biological effectiveness based on the absorptive properties of pure ocean water plus the added absorption and scattering of dissolved and suspended materials. Z_{10} is primarily determined by the inherent optical properties of the oceanic waters. Figure 5(a) and 5(b) show the Z_{10} maps for 310 and 380 nm, respectively. Both maps have the distinct features of the chlorophyll concentration distribution shown in Fig. 2(c). The ten percent depth is deeper for 380 nm band than for 310 nm band. In the oligotrophic regions of the oceans where chlorophyll concentrations are very low (0.01 to 0.1 mg/m^3), the Z_{10} depth varies from 50 to 70 meters for 380 nm band and from 20 to 30 meters for 310 nm band. On the other hand, in the regions of the globe where the chlorophyll concentration is very high, for example, in the north Atlantic where chlorophyll concentration is often greater than 1.0 mg/m^3 , the Z_{10} depth is less than 20 meters for 380 nm band and less than 5 meters for 310 nm band. Both $Z_{10}(380)$ and $Z_{10}(310)$ depths show a seasonal variation that is similar to the variation in chlorophyll concentration with season. For example, we find that in the south Pacific gyre where chlorophyll concentration is very small, the $Z_{10}(380)$ depth in January varies from 70 to 80 meters. The depth decreases slowly through April and by July it varies from 50 to 60 meters. The penetration depth then increases with time and by October varies from 70-80 meters. Similarly, in the North Atlantic, the $Z_{10}(380)$ depth in January varies from 20-30 meters in some regions and from 30-40 in other regions. In April, practically the entire region has value between 20-30 meters. By July, the value is between 10-20 meters and stays in this range through October. The maximum decrease occurs between April and July and maximum increase occurs between October and January. $Z_{10}(310)$ depths also show similar pattern and seasonal behavior. In general, the magnitude of the range of variation is approximately one-half of $Z_{10}(380)$.

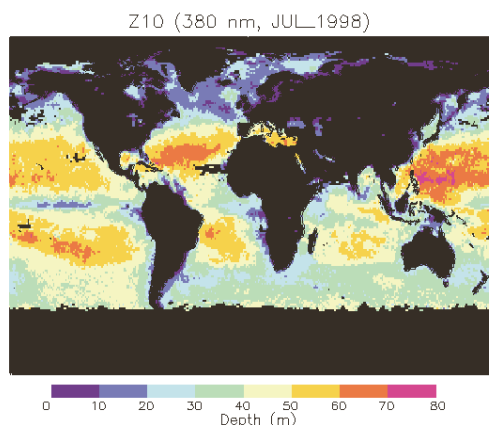


Fig 5 (a) Ten percent penetration depth (Z10) at 380 nm for the month of July 1998.

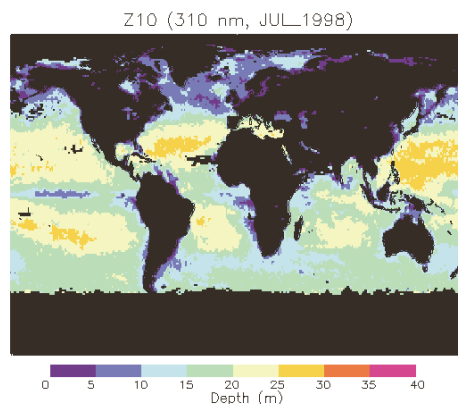


Fig 5 (a) Ten percent penetration depth (Z10) at 310 nm for the month of July 1998.

4.0 SUMMARY AND CONCLUSIONS

We have used our recently developed coupled ocean-atmosphere radiative transfer code to study seasonal variation of UV radiation in the ocean under clear and cloudy conditions. The calculations are from a combination of a UV-modified version of Hydrolight program (Mobley¹⁹) and a vector atmospheric radiative transfer code of Ahmad and Fraser²⁰. Inputs to the ocean-atmosphere calculations were TOMS' daily scene reflectivity and total ozone amount, and monthly chlorophyll concentrations from SeaWiFS on a $1^\circ \times 1^\circ$ grid. Monthly mean maps of E_d , K_d and Z_{10} were generated from seven days of mid-month daily data of the TOMS and monthly chlorophyll concentration from the SeaWiFS instruments. Our simulation results show that the seasonal variation of the surface UV irradiance in the UV-A part of the spectrum is primarily determined by the solar declination angle and then the degree of cloud cover. Clouds in general decrease the direct and diffuse solar irradiance, while non-absorbing aerosols (and very thin clouds) tend to increase the diffuse irradiance and decrease the direct component. However, the total downwelling irradiance decreases with aerosol and cloud optical thickness. In the UV-B part of the spectrum, the downwelling irradiances are further modulated by strong absorption by ozone in the atmosphere. At 5 meters depth, the downwelling irradiances are further modulated by the chlorophyll absorption. Maps of E_d at 5 meters depth show that the general features are similar to chlorophyll concentration maps and vary in general with the solar declination.

Our computed values of K_d 's are consistent with the chlorophyll values over the globe. That is, they are relatively small in the region of the oceans where the chlorophyll values are small and relatively high where the chlorophyll values are high. Also, our computed values of K_d (310) for three locations in the north Atlantic and Gulf of Mexico are in good agreement with those reported by Hojerslev and Aas³⁶. We also find that K_d (310) varies linearly with K_d (380) and the relationship agrees with observations summarized by Diaz et al³⁷.

Our Z_{10} penetration depths are also consistent with chlorophyll concentration distribution. Both $Z_{10}(380)$ and $Z_{10}(310)$ depths are large in the regions of low chlorophyll concentration and small in regions of high chlorophyll values in the ocean. In general, $Z_{10}(310)$ depths are one-half of $Z_{10}(380)$ depths and, like chlorophyll concentration, show a distinct seasonal variation.

REFERENCES

1. J. R. Herman, P. K. Bhartia, J. Ziemke, Z. Ahmad, and D. Larko, "UV-B radiation increases (1979-1992) from decreases in total ozone", *Geophys. Res. Lett.*, 23, 2117-2120, 1996.
2. J. R. Herman, R. D. Piacentini, J. Ziemke, E. Celarier, and D. Larko, "Interannual Variability of Ozone and UVB Ultraviolet Exposure", *J. Geophys. Res.*, 105, 29189-29194, 2000.

3. S. de Mora, S. Demers, and M. Vernet (Eds.), *"The effects of UV radiation in the marine environment,"* Cambridge Univ. Press, Cambridge, 2000.
4. K. R. Arrigo, D. Lubin, G. L. van Dijken, O. Holm-Hansen, and E. Morrow, "The Impact of a Deep Ozone Hole on Southern Ocean Primary Production", submitted to *J. Geophys. Res.*, 2003.
5. R. C. Smith, B.B.Prezelin, K.S.Baker, R.R.Biligare, N.P.Boucher, T.Coley, D.Karentz, S.MacIntyre, H.A.Matlic, D.Menzies, M.Ondrusek, Z.Wan, K.J.Waters, "Ozone depletion: ultraviolet radiation and phytoplankton biology in Antarctic waters", *Science*, 255, 952-959, 1992.
6. P. J. Neale, R. A. Davis, and J. J. Cullen, "Interactive effects of ozone depletion and vertical mixing on photosynthesis of Antarctic phytoplankton", *Nature*, 392, 585-589, 1998.
7. P. J. Neale, J. J. Cullen, and R. F. Davis, "Inhibition of marine photosynthesis by ultraviolet radiation: Variable sensitivity of phytoplankton in the Weddell-Scotia Sea during the austral spring". *Limnol. Oceanogr.*, 43, 433-448, 1998.
8. O. Holm-Hansen, D. Lubin, and E.W. Helbling, "Ultraviolet radiation and its effects on organisms in aquatic environments", in *Environmental UR Photobiology*, edited by A.R. Young et al; pp. 379-425, Plenum Press, New York, 1993.
9. K. R. Arrigo, "The impact of ozone depletion on phytoplankton growth in the Southern Ocean: Large-scale spatial and temporal variability", *Marine Ecology Progress Series* 114, 1-12, 1994.
10. R. G. Zepp, and M. O. Andreae, "Factors affecting the photochemical formation of carbonyl sulfide in seawater", *Geophys. Res. Lett.*, 1994.
11. P. J. Crutzen, "The possible importance of CSO for the sulfate layer of the stratosphere", *Geophys. Res. Lett.*, 3, 73-76, 1976.
12. A. Engel, and Schmidt, U., "Vertical profile measurements of carbonylsulfide in the stratosphere", *Geophys. Res. Lett.*, 21, 2219-2222, 1994.
13. R. J. Charlson, J. Langner, and H. Rodhe, "Sulphate aerosol and climate", *Nature* 348, 22, 1990.
14. N. A. Krotkov, P. K. Bhartia, J. R. Herman, V. Fioletov, and J. Kerr, "Satellite estimation of spectral surface UV irradiance in the presence of tropospheric aerosols 1: Cloud free case", *J. Geophys. Res.*, 103, 8779-879, 1998.
15. N. A. Krotkov, J. R. Herman, P. K. Bhartia, Z. Ahmad, V. Fioletov, "Satellite estimation of spectral surface UV irradiance 2: Effect of horizontally homogeneous clouds", *J. Geophys. Res.*, 106, 11743-11759, 2001.
16. J. R. Herman, S. McKenzie, S. Diaz, J. Kerr, S. Madronich, and G. Seckmeyer, "UV Radiation at the Earth's Surface", Chapter 9, 1999. UNEP/WMO Scientific Assessment of Ozone Depletion, 1999, edited by D. L. Albritton, R. T. Watson, and P. J. Aucamp. *WMO Global Ozone Res. And Monit. Proj.*, Geneva, 1999.
17. J. R. Herman, N. A. Krotkov, E. A. Celarier, D. Larko, and G. Labow, "The distribution of UV radiation at the Earth's surface from TOMS measured UV-backscattered radiances", *J. Geophys. Res.*, 104, 12,059-12,076, 1999.
18. T. F. Eck, P.K.Bhartia, and J.B.Kerr, "Satellite estimation of spectral UVB irradiance using TOMS derived total ozone and UV reflectivity", *Geophys. Res. Lett.*, 22, 611-614, 1995.
19. C. D. Mobley, *"Light and Water: Radiative Transfer in Natural Waters,"* Academic Press, San Diego, 592 pp., 1994.
20. Z. Ahmad, and R. S. Fraser, "An iterative radiative transfer code for ocean-atmosphere systems", *J. Atmos. Sci.*, 39, 656-665, 1982.
21. A.P. Vasilkov, J. Herman, Z. Ahmad, M. Kahru, B.G. Mitchell, and M. Tzortziou, "A comparison of UV penetration into ocean waters with models and *in situ* data," in *Proceedings of the Ocean Optics XVI Conference*, 18-22 November 2002, Santa Fe, NM, USA, 2002.
22. M. Kahru and B. G. Mitchell, "Spectral reflectance and absorption of a massive red tide off Southern California", *J. Geophys. Res.*, 103, 21601-21609, 1998.

23. A. P. Vasilkov, N. Krotkov, J.R. Herman, C. McClain, K. Arrigo, and W. Robinson, "Global mapping of underwater UV irradiance and DNA-weighted exposures using TOMS and SeaWiFS data products," *J. Geophys. Res.*, 106, 27205-27219, 2001.
24. AFGL, "*Handbook of Geophysics and Space Environment*", Adolph S. Jursa (Ed.), Air force Geophysics Laboratory, 1985
25. A. M. Bass and R. J. Paur, "The ultraviolet cross-section of ozone, I, Measurements", in *Atmospheric Ozone*, C. Z. Zeferos, and Ghazi (Eds.), pp 606-616, D. Reidel, Norwell, Mass.,1985.
26. G. E., Brueckner, et al., "The Solar Ultraviolet Spectral Irradiance Monitor (SUSIM) onboard the Upper Atmospheric Research Satellite (UARS)", *J. Geophys. Res.*, 98, 10,695-10,711, 1993.
27. C. Cox, and W. H. Munk, "The measurement of roughness of the sea surface from photographs of the sun glitter", *J. Opt. Soc. Amer.*, 44,838-850, 1954.
28. K. Stamnes, S.-C. Tsay, W. Wiscombe, and K. Jayaweera, "Numerically stable algorithm for discrete ordinate method radiative transfer in multiple scattering and emitting layered media", *Appl. Optics*, 27, 2502-2509, 1988.
29. D. Deirmendjian, *Electromagnetic scattering on spherical polydispersions*, Elsevier, 290, 1969.
29. Hansen, J.E., Multiple scattering of polarized light in planetary atmosphere. Part I. The doubling method, *J. Atmos. Sci.*, 36, 508,518, 1971.
30. King, M.D., and Harshvardhan, Comparative accuracy of the albedo, transmission and absorption for selected radiative approximation, *NASA Reference Publication* 1160, 1986.
31. W. B. Rossow, and R.A. Schiffer, "Advances in understanding clouds from ISCCP", *Bull. Amer. Meteor. Soc.*, 80, 2261-2287, 1999.
32. A. P. Vasilkov, J. Herman, N.A. Krotkov, M. Kahru, B.G. Mitchell, and C. Hsu, "Problems in assessment of the UV penetration into natural waters from space-based measurements," *Optical Engineering*, 3019-3027, 41, 2002.
33. R. M. Pope and E. S. Fry, "Absorption spectrum (380-700 nm) of pure water. 11. Integrating cavity measurements," *Appl. Opt.* 36, 8710-8723 (1997).
34. T. I. Quickenden and J. A. Irvin, "The ultraviolet absorption spectrum of liquid water," *J. Chem. Phys.* 72, 4416-4428 (1980).
35. R.C. Smith and K.C.Baker, "Optical properties of the clearest natural waters," *Appl. Opt.*, 20, 177-186, 1981.
36. N. K. Hojerslev, and E. Aas, "A relationship for the penetration of ultraviolet B radiation into the Norwegian sea", *J. Geophys. Res.*, 96, 17003-17005, 1991.
37. S. B Diaz, J. H. Morrow and C. R. Booth, "UV physics and optics", in *The effects of UV radiation in the marine environment*, S. de Mora, S. Demers and M. Vernet (Eds.), Cambridge environmental chemistry series-10, Cambridge University Press, 2000.